IET Electric Power Applications

Research Article

IET Journals
The Institution of Engineering and Technology

Novel repulsive magnetic bearing flywheel system with composite adaptive control

ISSN 1751-8660
Received on 6th June 2018
Revised 19th November 2018
Accepted on 5th December 2018
E-First on 6th February 2019
doi: 10.1049/iet-epa.2018.5312
www.ietdl.org

Sinan Basaran[1] ✉, *Selim Sivrioglu*[2]

[1]*Department of Mechanical Engineering, Bilecik Seyh Edebali University, Bilecik 11230, Turkey*
[2]*Department of Mechanical Engineering, Gebze Technical University, Gebze 41400, Turkey*
✉ *E-mail: sinan.basaran@bilecik.edu.tr*

Abstract: Here, a novel flywheel structure is proposed with passive permanent magnet (PM) bearings in the radial and axial directions and an active magnetic bearing (AMB) in the axial direction. In the proposed structure, passive magnetic bearings do not provide a stable magnetic levitation in all directions, but it is possible to maintain the dynamic stability of the flywheel by using AMB in the axial direction. In the proposed bearing structure, radial repulsive magnetic bearings (RMBs) reduce the power consumption with less complexity in the bearing structure but impose disturbance forces that deteriorate the stability of the actively controlled flywheel system. A complete model of the flywheel system is derived and transformed for a control design. A Lyapunov-based composite adaptive feedback control is designed for maintaining the stability under disturbances and a close convergence to the desired trajectory with fast parameter estimation. The performance of the composite adaptive control was experimentally verified for different cases using the RMB flywheel system. Additionally, a PID control was experimentally verified to demonstrate the usefulness of parameter estimation.

1 Introduction

A spinning flywheel has interesting features as an engineering system. It stores rotational kinetic energy and produces angular momentum. They can potentially be used in energy storage systems and an attitude control actuator in space applications [1–4]. In most conventional systems, flywheels are supported by ball bearings. Unlike conventional mechanical bearings, magnetic bearings provide non-contact, frictionless, and oil-free mechanical motion between the rotating body and bearing with high precision [5–9]. This technology has mainly two types of bearing structures such as active magnetic bearings (AMBs) and passive magnetic bearings (PMBs). PMB is using repulsive forces of the PMs; hence, they are known as a repulsive magnetic bearing (RMB) in the literature. Combination of these two bearing is called hybrid magnetic bearings (HMBs). An HMB is used to combine advantages of both AMB and PMB. There are different types of HMB structures. PM-biased axial HMB is investigated in [10]. The HMB in [10] can simultaneously control axial translation and the radial tilt. In traditional approach, using an axial magnetic bearing is a simple way but can control only axial translation of the motion. In [11], for providing the radial suspension, PMs are used. Using the PMs in HMB systems gives disturbance load on levitation object. Actively controlled electromagnets can stabilise the disturbance forces of the system [12].

An AMB uses electromagnets to generate attractive forces with a feedback control. The AMBs have advantages over conventional mechanical bearings such as adjustment of stiffness and damping values of the bearing. Therefore, disturbance forces acting on the suspended object are effectively cancelled with the control of the AMB. On the other hand, AMBs consume energy and need a feedback control in operation. An RMB uses repulsive magnetic force generated by PMs for a magnetic levitation [13–17]. According to the Earnshaw theorem, a stable magnetic levitation is impossible in a system composed solely of PMs. An RMB is usually combined with a mechanical guidance or actively controlled electromagnets for a stable levitation due to instability at least one direction. It is an advantage that no energy is required to generate levitation force and larger rotor–stator gaps are possible in this type of bearings [18–20].

Conventional axial magnetic bearings have a single winding coil to support the disk. Thus, the axial bearing can only limit linear displacements in the z-axis. On the other hand, the angular displacement of the disk cannot be controlled by the conventional axial bearing. In the proposed structure, four electromagnet sets can be controlled independently. Unlike the conventional axial magnetic bearing, angular movements of the flywheel can be controlled by the proposed axial magnetic bearing. In this study, a flywheel system is designed with an arrangement of PMs in both radial and axial directions. In the proposed structure, while the radial RMBs provide a passive levitation of the flywheel in the radial directions, an active axial magnetic bearing ensure the stability of the flywheel system in the axial direction [21]. The proposed axially active controlled flywheel reduces the power consumption due to passive levitation of the radial directions.

In the proposed magnetic bearing structure, the flywheel system is subjected to considerable disturbance loads due to the unstable forces of the PMs. To achieve a stable levitation, the axial AMB should have a suitable feedback control. Also, it should be better to choose controllers that adapt itself to changing conditions. The classical adaptation control methods use state feedback error for adaptation rule of the parameters. To achieve a faster parameter estimation, the adaptive controller should include a specialised additional least-squares estimation term. The proposed Lyapunov-based composite full state feedback controller gives a faster parameter estimate convergence and utilises an update rule to achieve the stable levitation of the RMB system.

The paper is organised as follows: Section 2 gives the derivation of the dynamic equations of the axial and radial repulsive bearings. Section 3 presents a complete modelling of the flywheel system with RMBs. Moreover, Section 4 gives the proposed control design formulation in detail. Finally, the experimental implementation of the designed controller for different case studies and conclusions are presented in Sections 5 and 6.

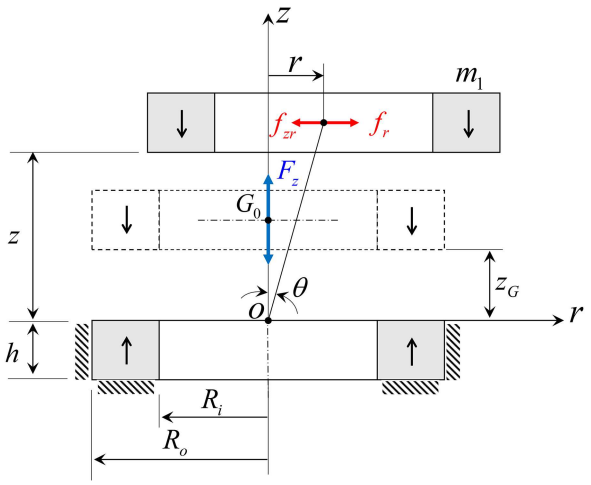

Fig. 1 *Axial repulsive bearing dynamics*

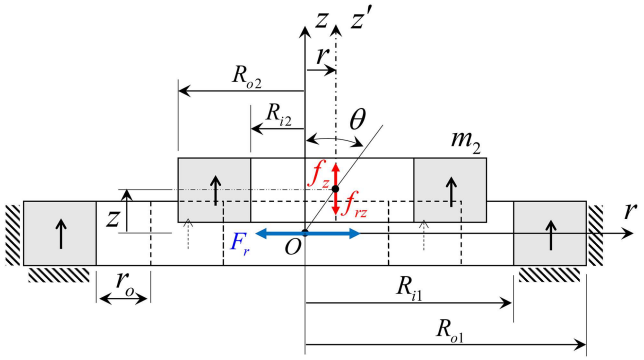

Fig. 2 *Radial repulsive bearing dynamics*

2 Modelling of magnetic bearings

2.1 Axial RMB

The dynamic equations of the axial RMB can be derived using Bassani's study [22]. Consider an axial RMB as shown in Fig. 1 with equal rings of mass m_1 and with opposite fields B_r. The upper PM ring is initially levitated over the fixed PM ring by an axial stable force F_z at a height z_G. The equation of motion in the axial direction for the levitated ring PM is given by

$$m_1\ddot{z} + F_z = 0 \tag{1}$$

where the axial stable force is a vibrating characteristic such as $F_z = F_{zG}\cos\Omega_z t$ and the natural frequency is $\Omega_z = \sqrt{K_z/m_1}$. Here, K_z is the axial stiffness. Since levitation force is alternating, the axial displacement has the same characteristics $z = z_G\cos\Omega_z t$.

While the axial stable force acts at the levitation centre of G_0, the upper PM is moved laterally by the radial unstable force f_r. The upper PM is moved to its new position of the axial z and the radial r distances by these forces. The opposed shifting force f_{zr} is generated due to the axial stable vibrating force. The radial equation of motion of the upper ring PM is given by

$$m_1\ddot{r} + f_r - f_{zr} = 0 \tag{2}$$

where $f_{zr} = F_z\sin\theta$. Arranging (2) by taking $f_r = (-K_z/2)r$, $\theta \cong r/z$, and $F_z\sin\theta = (K_z\cos\Omega_z t)r$ gives

$$m_1\ddot{r} - \left(\frac{1}{2}K_z + K_z\cos\Omega_z t\right)r = 0 \tag{3}$$

The radial dynamics of the axial repulsive bearing obtained (3) has unstable characteristics due to negative stiffness effect. The dynamic equations obtained in (1) and (3) showed that the axial RMB has the axial stability and radial instability.

2.2 Radial RMB

For the radial RMB having two ring PMs nested as depicted in Fig. 2, the radial and axial dynamic equations can be derived using the same approach given in [22]. The inner PM ring is initially levitated inside the fixed PM ring by a radial stable force F_r with a nominal gap r_0. In this situation, the radial stable force F_r acts at the levitation centre O. The equation of motion in the radial direction for the levitated inner ring PM is given by

$$m_2\ddot{r} + F_r = 0 \tag{4}$$

where the radial stable force and the natural frequency are $F_r = F_{rO}\cos\Omega_r t$ and $\Omega_r = \sqrt{K_r/m_2}$. Here, K_r is the radial stiffness. The inner PM is moved vertically from the initial position by the axial unstable force f_z. An opposing force f_{rz} is also generated by the radial stable force. The axial dynamics of the inner ring PM is obtained as

$$m_2\ddot{z} + f_z - f_{rz} = 0 \tag{5}$$

where $f_{rz} = F_r/\tan\theta$. Substituting $f_z = (-K_r/2)z$, $\theta \cong r/z$, and $F_r/\tan\theta = (K_r\cos\Omega_r t)z$ into (5), the final form of the axial dynamic equation is derived as

$$m_2\ddot{z} - \left(\frac{1}{2}K_r + K_r\cos\Omega_r t\right)z = 0 \tag{6}$$

Considering the dynamics obtained in (4) and (6), the radial RMB has the radial stability and axial instability characteristics.

2.3 Axial AMB

The electromagnetic forces generated by the axial AMB electromagnets can be written as a function of coil current and air gap as follows:

$$f_{z_j} = K\frac{i_{z_j}^2}{(z_0 - z_j)^2}, \quad j = 1, \ldots, 4 \tag{7}$$

where i_{z_1}, i_{z_2}, i_{z_3}, and i_{z_4} are control currents applied to electromagnets through the power amplifier. Also, z_0 is the gap between the flywheel and electromagnets. Moreover, K is the magnetic force coefficient and given as $K = \mu_0 N^2 A_a/4$.

Conventional axial magnetic bearings have a single winding coil to limit the displacement of a disk connected to the main rotor. In this type of arrangement, the disk cannot be controlled angularly due to tilted sideways. In the proposed flywheel system, unlike conventional axial magnetic bearing, we use four separate electromagnets that can be controlled independently by using individual power amplifiers. Note that Fig. 3 shows two electromagnets in the *Gxz* plane and the other two electromagnets are in the *Gyz* plane. The proposed axial bearing structure allows the flywheel to follow the tilted trajectory besides the setpoint trajectory. Therefore, a non-linear control application is possible to suspend the flywheel. Depending on the flywheel dynamics, the axial active bearing may generate different electromagnetic forces.

3 Modelling of the flywheel system

3.1 Flywheel system structure

The proposed RMB flywheel system structure is schematically shown as a cross-section in Fig. 3. The upper and lower PM bearings operating in the repulsion mode have a special structure. As seen in Fig. 3, while *A*1 (ring PMs) and *A*2 (disk PMs) pairs generate axial levitation forces, *R*1 and *R*2 ring PM pairs create radial levitation forces. For these bearings, a screw mechanism for the outer ring that moves the outer PMs to the centre of the inner PM centre position is used to set the initial position and eliminate the misalignment issue. In the proposed design, axially magnetised two pairs of PMs are selected for the inner and outer rings (*R*1 and

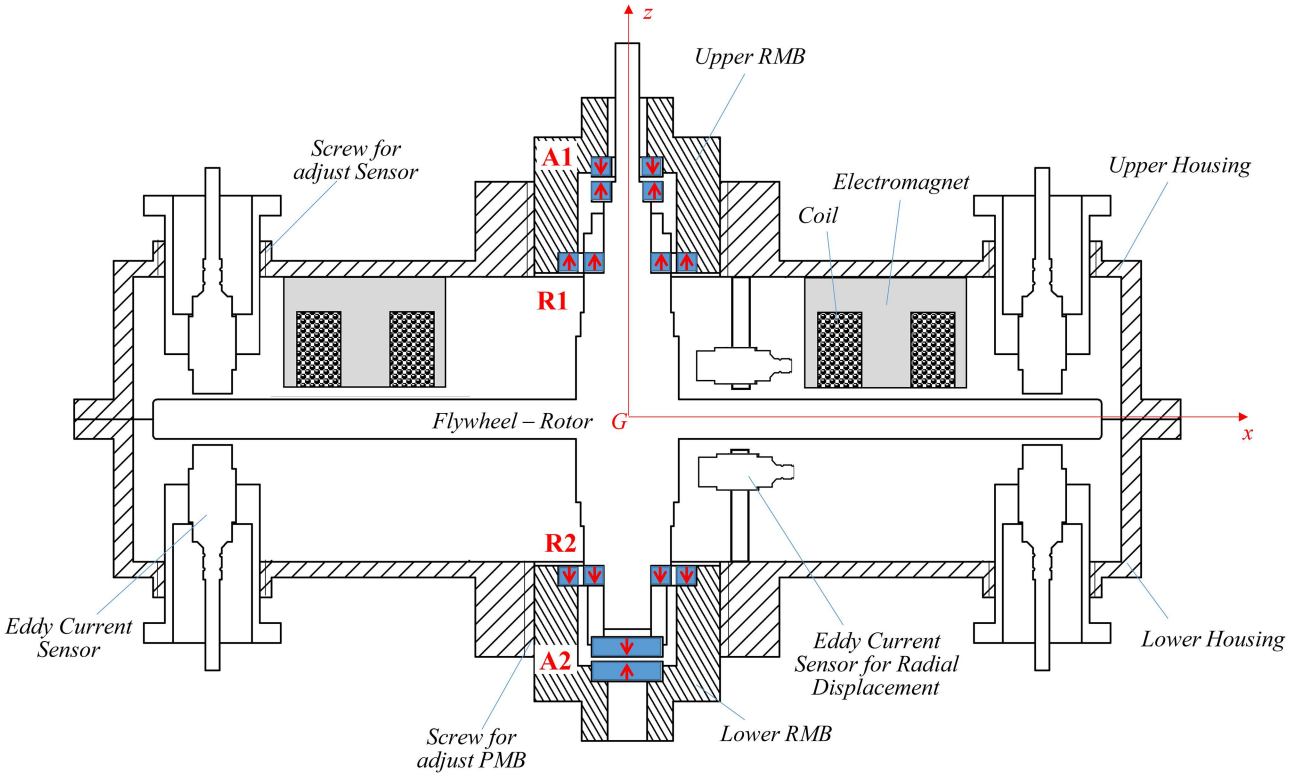

Fig. 3 *Cross-section view of the flywheel-RMB system*

*R*2). The poles of the PMs are oriented to repel each other inside the inner and the outer rings. This type of structure is discussed in many different research works [21–24].

In the proposed novel RMB flywheel system, control approach is utilised for stabilisation by using an active axial magnetic bearing which has four electromagnets. Also, eddy current sensors located in the vertical direction for a feedback control. Moreover, to observe the radial movement of the rotor, two eddy current sensors are also attached to the system at the upper and lower side of the rotor, although there is no control in the radial direction. The proposed flywheel system has a complete symmetry inside the housing. Note that an electric motor would be integrated for future work to rotate the flywheel using a magnetic coupling without any contact at the top of the rotor.

3.2 Derivation of equation of motion

The flywheel-RMB system structure for modelling is depicted schematically in Fig. 4 with respect to the *Gxz* plane. Owing to symmetry, the *Gyz* plane has also the same structure and the centre of mass *G* of the flywheel system is known. The flywheel is assumed to be rigid and has translational motions in *x*, *y*, and *z* directions and angular motions η_x and η_y around *x* and *y* axes, respectively. All the necessary physical parameters are shown in Table 1. RMBs produce magnetic forces that act radially and axially on the rotor. The effecting forces generated by each axial and radial repulsive bearings are shown in Fig. 4. The radial dynamics of the flywheel is written as

$$m_{\mathrm{f}}\ddot{x}_g + F_{x2} + F_{x3} + f_{x1} - f_{zx1} + f_{x4} - f_{zx4} = 0 \tag{8}$$

where x_g is the radial displacement of the flywheel centre of the mass. Substituting and arranging the RMB forces according to Sections 2.1 and 2.2, (8) becomes

$$m_{\mathrm{f}}\ddot{x}_g + \left[K_{x2} + K_{x3} - K_{z1}\left(\frac{1}{2} + \cos\Omega_{z1}t\right) - K_{z4}\left(\frac{1}{2} + \cos\Omega_{z4}t\right)\right]x_g = 0 \tag{9}$$

Finally, the radial dynamics is expressed as

$$m_{\mathrm{f}}\ddot{x}_g + \sum K_R x_g = 0 \tag{10}$$

where K_R is the total radial stiffness. For stability in the radial direction, the following condition must be maintained

$$\sum K_R > 0 \tag{11}$$

In this study, the radial repulsive bearings *R*1 and *R*2 are designed to satisfy the condition defined in (11). In the *y* direction, the following equation of motion can be written similarly as

$$m_{\mathrm{f}}\ddot{y}_g + \sum K_R y_g = 0 \tag{12}$$

The axial dynamics of the flywheel is derived as

$$m_{\mathrm{f}}\ddot{z}_g - F_{z1} + F_{z4} + f_{z2} - f_{xz2} + f_{z3} - f_{xz3} = f_{a1} + f_{a2} + f_{a3} + f_{a4} \tag{13}$$

where z_g is the axial displacements of the flywheel centre of the mass. Also f_{a1}, f_{a2}, f_{a3}, and f_{a4} show electromagnetic forces generated by the electromagnets. Substituting the forces in (13)

$$m_{\mathrm{f}}\ddot{z}_g + (K_{z4} - K_{z1})z_g - \left(K_{x2}\left(\frac{1}{2} + \cos\Omega_{x2}t\right) + K_{x3}\left(\frac{1}{2} + \cos\Omega_{x3}t\right)\right)z_g = \sum_{j=1}^{4} f_{aj} \tag{14}$$

The final form of (14) is obtained as

$$m_{\mathrm{f}}\ddot{z}_g + K_z z_g = \sum_{j=1}^{4} f_{aj} + F_{\mathrm{d}} \tag{15}$$

where

$$K_z = K_{z4} - K_{z1} \tag{16}$$

and

$$F_{\mathrm{d}} = [K_{x2}(0.5 + \cos\Omega_{x2}t) + K_{x3}(0.5 + \cos\Omega_{x3}t)]z_g\,. \tag{17}$$

A positive vertical stiffness is possible by selecting the $A1$ and $A2$ repulsive bearings such as $K_{z4} > K_{z1}$. Satisfying this condition, it is also possible to take the weight load of the flywheel by the axial repulsive bearing $A2$. The levitation of the axial direction is not stable due to the disturbance force F_{d} generated by radial repulsive bearings. In this study, actively controlled electromagnets are aimed to stabilise the flywheel-repulsive bearing under the disturbance force F_{d}.

The angular dynamics η_y of the flywheel-RMB system is obtained as

$$\begin{aligned} &J_{\mathrm{f}}\ddot{\eta}_y - J_p\omega\dot{\eta}_x + F_{x2}L_m + F_{x3}L_m + f_{x1}L_p - f_{zx1}L_p \\ &\quad + f_{x4}L_p - f_{zx4}L_p = f_{a1}L_{\mathrm{f}} - f_{a2}L_{\mathrm{f}} \end{aligned} \tag{18}$$

Inserting the radial and axial repulsive bearing forces, (18) becomes

$$\begin{aligned} &J_{\mathrm{f}}\ddot{\eta}_y - J_p\omega\dot{\eta}_x + (K_{x2} + K_{x3})L_m^2\,\eta_y \\ &\quad - K_{z1}L_p^2\left(\frac{1}{2} + \cos\Omega_{z1}t\right)\eta_y - K_{z4}L_p^2\left(\frac{1}{2} + \cos\Omega_{z4}t\right)\eta_y \\ &\quad = f_{a1}L_{\mathrm{f}} - f_{a2}L_{\mathrm{f}} \end{aligned} \tag{19}$$

Arranging (19), a final form is obtained as

$$\begin{aligned} &J_{\mathrm{f}}\ddot{\eta}_y - J_p\omega\dot{\eta}_x + \left(K_R L_m^2 - \frac{1}{2}K_A L_p^2\right)\eta_y \\ &\quad - (K_A\cos\Omega_A t)L_p^2\eta_y = f_{a1}L_f - f_{a2}L_{\mathrm{f}} \end{aligned} \tag{20}$$

where

$$\begin{aligned} &K_A(0.5 + \cos\Omega_A t)L_p^2 = [K_{z1}(0.5 + \cos\Omega_{z1}t) \\ &+ K_{z4}(0.5 + \cos\Omega_{z4}t)]L_p^2 \end{aligned}$$

is the equivalent stiffness and $K_R = K_{x2} + K_{x3}$. Similarly, the angular dynamics of η_x can be derived as follows:

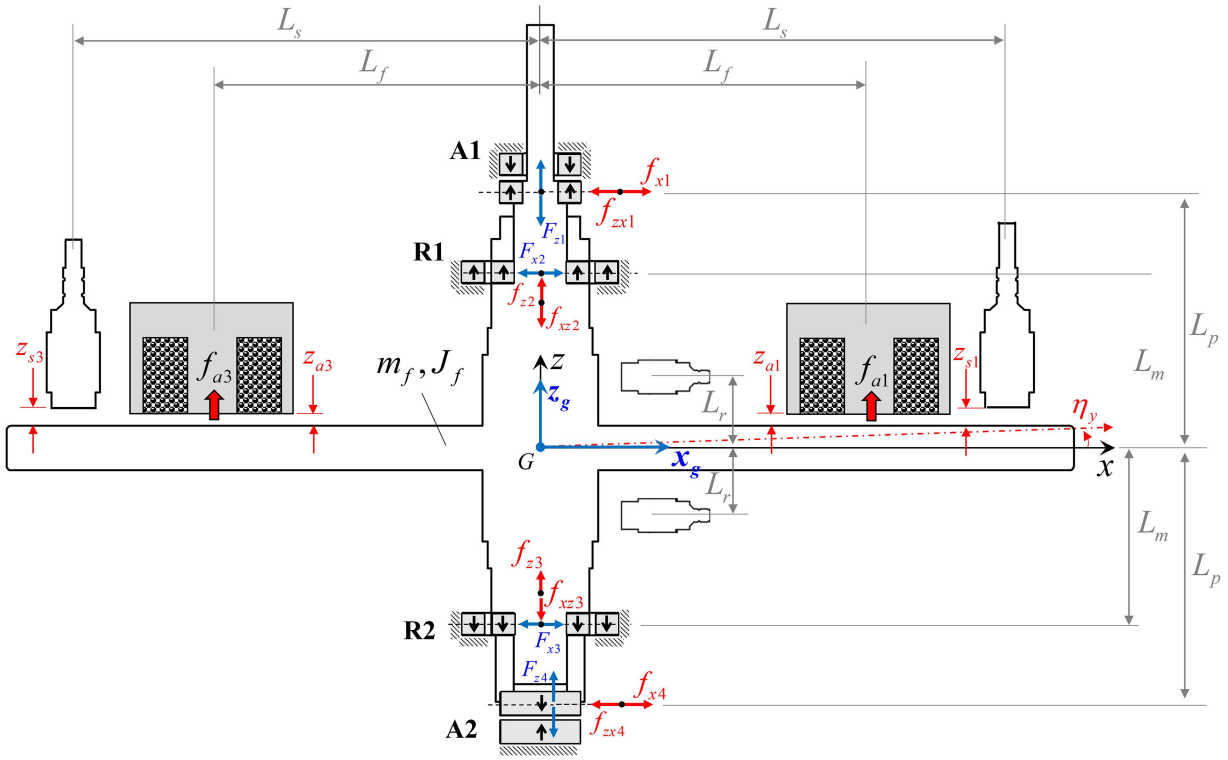

Fig. 4 *Structure of the RMB flywheel system for modelling*

Table 1 Values of the parameters for the flywheel system

Symbol	Value	Unit	Meaning
m_{f}	2.2215	kg	mass of the flywheel
J_{f}	76.3374×10^{-4}	kgm^2	moment of the inertia of the flywheel
J_p	148.0760×10^{-4}	kgm^2	polar moment of inertia
K_R	13368	N/m	radial stiffness of the RMB at equilibrium state
K_A	21148	N/m	axial stiffness of the RMB at equilibrium state
L_m	39.5×10^{-3}	m	the distance from the flywheel centre of the mass to the RMB
L_p	60.625×10^{-3}	m	the distance from the flywheel centre of the mass to the RMB
L_s	105×10^{-3}	m	the distance from the flywheel centre of mass to eddy current sensors
L_r	15×10^{-3}	m	the distance from the flywheel centre of mass to eddy current sensors
z_0	1×10^{-3}	m	initial air gap
μ_0	$4\pi \times 10^{-7}$	H/m	magnetic field constant
N	250	—	number of coil turns
A_a	3.1416×10^{-4}	m^2	the cross-sectional area of the electromagnet

$$J_f\ddot{\eta}_x + J_p\omega\dot{\eta}_y + \left(K_R L_m^2 - \frac{1}{2}K_A L_p^2\right)\eta_x - (K_A\cos\Omega_A t)L_p^2\eta_x = f_{a3}L_f - f_{a4}L_f \tag{21}$$

3.3 Transform of equations

The equations of motion given in (10), (12), (14), (20), and (21) are derived according to the centre of mass of the flywheel. Since the repulsive bearings in the radial directions are stable, only the axial direction will be controlled by an AMB. To have a suitable mathematical model for the proposed control design, it is necessary to transform (17), (20), and (21) from the centre of mass to the actuator locations [25]. The transformed displacements are defined as

$$\begin{aligned} z_{a1} &= z_g - L_f\eta_y \\ z_{a2} &= z_g + L_f\eta_y \\ z_{a3} &= z_g - L_f\eta_x \\ z_{a4} &= z_g + L_f\eta_x \end{aligned} \tag{22}$$

where z_{a1}, z_{a2}, z_{a3}, and z_{a4} are the displacements of the flywheel at the electromagnetic actuator locations in z direction. Here, z_g show the vertical displacements of the rotor centre of mass. Defining the angles $\eta_y = (z_{a2} - z_{a1})/2L_f$ and $\eta_x = (z_{a3} - z_{a4})/2L_f$, the dynamical equations from the centre of mass to the actuator locations are transformed and written in the matrix form as follows:

$$\begin{aligned} &\begin{bmatrix} -\frac{J_f}{2L_f} & \frac{J_f}{2L_f} & 0 & 0 \\ 0 & 0 & \frac{J_f}{2L_f} & -\frac{J_f}{2L_f} \end{bmatrix}\begin{bmatrix} \ddot{z}_{a1} \\ \ddot{z}_{a2} \\ \ddot{z}_{a3} \\ \ddot{z}_{a4} \end{bmatrix} \\ &+\begin{bmatrix} 0 & 0 & -\frac{J_p\omega}{2L_f} & \frac{J_p\omega}{2L_f} \\ -\frac{J_p\omega}{2L_f} & \frac{J_p\omega}{2L_f} & 0 & 0 \end{bmatrix}\begin{bmatrix} \dot{z}_{a1} \\ \dot{z}_{a2} \\ \dot{z}_{a3} \\ \dot{z}_{a4} \end{bmatrix} \\ &+\begin{bmatrix} K_1 & K_2 & 0 & 0 \\ 0 & 0 & K_3 & K_4 \end{bmatrix}\begin{bmatrix} z_{a1} \\ z_{a2} \\ z_{a3} \\ z_{a4} \end{bmatrix} \\ &=\begin{bmatrix} L_f & -L_f & 0 & 0 \\ 0 & 0 & L_f & -L_f \end{bmatrix}\begin{bmatrix} f_{a1} \\ f_{a2} \\ f_{a3} \\ f_{a4} \end{bmatrix} \end{aligned} \tag{23}$$

where elements of the stiffness matrix are

$$K_1 = K_4 = \frac{-K_s + (K_A\cos\Omega_A t)L_p^2}{2L_f},$$

$$K_2 = K_3 = \frac{K_s - (K_A\cos\Omega_A t)L_p^2}{2L_f}, \quad \text{and}$$

$$K_s = K_R L_m^2 - \frac{1}{2}K_A L_p^2.$$

A compact form of (23) can be written as

$$\boldsymbol{M}\ddot{\boldsymbol{z}}_a + \boldsymbol{C}(\omega)\dot{\boldsymbol{z}}_a + \boldsymbol{K}\boldsymbol{z}_a = \boldsymbol{F}\boldsymbol{u} \tag{24}$$

where $\boldsymbol{z}_a = \begin{bmatrix} z_{a1} & z_{a2} & z_{a3} & z_{a4} \end{bmatrix}^{\mathrm{T}}$ and $\boldsymbol{u} = \begin{bmatrix} f_{a1} & f_{a2} & f_{a3} & f_{a4} \end{bmatrix}^{\mathrm{T}}$ are the displacement and force vectors, respectively. Also, $\boldsymbol{M} \in \mathbb{R}^{n\times 4}$ is the positive-definite mass matrix, $\boldsymbol{C} \in \mathbb{R}^{n\times 4}$ is the damping matrix, $\boldsymbol{K} \in \mathbb{R}^{n\times 4}$ is the stiffness matrix, and $\boldsymbol{F} \in \mathbb{R}^{n\times 4}$ is the force matrix. Note that $n = 2$ represents the angular dynamic equation of the system. The transformed dynamic equation can be written as follows:

$$\boldsymbol{F}^{+}\boldsymbol{M}\ddot{\boldsymbol{z}}_a + \boldsymbol{F}^{+}\boldsymbol{C}(\omega)\dot{\boldsymbol{z}}_a + \boldsymbol{F}^{+}\boldsymbol{K}\boldsymbol{z}_a = \boldsymbol{u} \tag{25}$$

Note that $\{\boldsymbol{F}^{+}\}$ represents the Moore–Penrose pseudoinverse of the matrix $\{\boldsymbol{F}\}$. The dynamic equation can also be defined as

$$\boldsymbol{F}^{+}\boldsymbol{M}\ddot{\boldsymbol{z}}_a + \boldsymbol{F}^{+}\boldsymbol{C}(\omega)\dot{\boldsymbol{z}}_a + \boldsymbol{F}^{+}\boldsymbol{K}\boldsymbol{z}_a = \boldsymbol{W}\boldsymbol{\Phi} \tag{26}$$

where $\boldsymbol{W} \in \mathbb{R}^{n\times p}$ is the regression matrix which contains system states and $\boldsymbol{\Phi} \in \mathbb{R}^{p}$ the system physical parameter vector

$$\boldsymbol{\Phi}^{\mathrm{T}} = \begin{bmatrix} \Phi_1 & \Phi_2 & \Phi_3 & \Phi_4 \end{bmatrix}^{\mathrm{T}} = \begin{bmatrix} J_f & J_p & K_R & K_A \end{bmatrix}^{\mathrm{T}} \tag{27}$$

4 Composite adaptive control design

In the proposed flywheel design, strong non-linearity and parametric uncertainties due to RMBs were appeared. To overcome such problems, we designed a composite adaptive control using the derived model of the flywheel. Adaptive control techniques allow a systematic approach for estimations of the system parameters in real time. It also provides stability against disturbance forces and a good convergence to the desired trajectory and parameter estimation. However, it is not always practical to use standard adaptation based on the persistence of excitation conditions. In this section, the modified adaptive control design is illustrated to ensure the asymptotic convergence of both the tracking error and the parameter estimation error. The asymptotic convergence of the parameter error is achieved if the infinite integral condition on the filtered regression matrix holds [26].

4.1 Force filtering

The first step in the formulation of the composite adaptive control is the constructing of a filtered regression matrix. The force can be filtered to eliminate the acceleration measurements. The dynamics of the system given in (26) can be written as follows:

$$\boldsymbol{u} = \boldsymbol{W}\boldsymbol{\Phi} \tag{28}$$

Equation (28) can also be expressed as

$$\boldsymbol{u} = \dot{\boldsymbol{h}} + \boldsymbol{g} \tag{29}$$

where $\dot{\boldsymbol{h}} = \mathrm{d}/\mathrm{d}t(\boldsymbol{F}^{+}\boldsymbol{M}\dot{\boldsymbol{z}}_a)$, $\boldsymbol{g} = -\dot{\boldsymbol{F}}^{+}\dot{\boldsymbol{M}}\dot{\boldsymbol{z}}_a + \boldsymbol{F}^{+}\boldsymbol{C}\dot{\boldsymbol{z}}_a + \boldsymbol{F}^{+}\boldsymbol{K}\boldsymbol{z}_a$. Note that $\dot{\boldsymbol{F}}^{+}\dot{\boldsymbol{M}} = 0$. In this way, the system dynamics have been separated, so that $\ddot{\boldsymbol{z}}_a$ could be eliminated. The filtered version of the force is defined as

$$\boldsymbol{u}_f = F_f * \boldsymbol{u} = F_f * \dot{\boldsymbol{h}} + F_f * \boldsymbol{g} \tag{30}$$

where F_f is the impulse response of a linear, strictly proper filter and $\{*\}$ denotes the convolution operator. By using the convolution property defined in the below equation

$$F_f * \dot{\boldsymbol{h}} = \dot{F}_f * \boldsymbol{h} + F_f(0)\boldsymbol{h} - F_f\boldsymbol{h}(0) \tag{31}$$

Equation (30) can be rewritten as in (32) by inserting the $\boldsymbol{h}$ and $\boldsymbol{g}$

$$\begin{aligned} \boldsymbol{u}_f = \dot{\boldsymbol{F}}_f * \left(F^{+}\boldsymbol{M}\dot{\boldsymbol{z}}_a\right) + F_f(0)\left(\boldsymbol{F}^{+}\boldsymbol{M}\dot{\boldsymbol{z}}_a\right) \\ -F_f\left(\boldsymbol{F}^{+}\boldsymbol{M}\dot{\boldsymbol{z}}_a(0)\right) + F_f\left(\boldsymbol{F}^{+}\boldsymbol{C}\dot{\boldsymbol{z}}_a + \boldsymbol{F}^{+}\boldsymbol{K}\boldsymbol{z}_a\right) \end{aligned} \tag{32}$$

where $\dot{F}_f$ is the impulse response of the filter. In practice, estimation is realised with difference variable as follows:

$$\tilde{\boldsymbol{u}}_f = \boldsymbol{W}_f\tilde{\boldsymbol{\Phi}} \tag{33}$$

where $\tilde{\boldsymbol{u}}_{\mathrm{f}} = \boldsymbol{u}_{\mathrm{f}} - \hat{\boldsymbol{u}}_{\mathrm{f}}$ and $\tilde{\boldsymbol{\Phi}} = \boldsymbol{\Phi} - \hat{\boldsymbol{\Phi}}$. Also, $\boldsymbol{W}_{\mathrm{f}} \in \mathbb{R}^{n \times p}$ is the filtered regression matrix. Here, $\tilde{\boldsymbol{\Phi}}$ denotes the parameter estimation error vector and $\hat{\boldsymbol{\Phi}}$ is a dynamic estimate of the unknown, constant, parameter vector of $\boldsymbol{\Phi}$.

4.2 Controller development

The position tracking error $\boldsymbol{e} = z_d - z_a$, $\boldsymbol{e}(t) \in \mathbb{R}^n$, and its double-time derivative is defined as follows:

$$\ddot{\boldsymbol{e}} = \ddot{\boldsymbol{z}}_d - \ddot{\boldsymbol{z}}_a \tag{34}$$

From the definition of the position tracking error, the control objective is to make $\boldsymbol{e}(t) \to 0$ as $t \to \infty$. In (34), the desired motion trajectory is specified such that $z_d(t)$ and its first two derivatives are all bounded functions of time [27]. In addition, a filtered tracking error $\boldsymbol{r} = \dot{\boldsymbol{e}} + \boldsymbol{\alpha e}$, $\boldsymbol{r}(t) \in \mathbb{R}^n$, and its time derivative is defined as follows:

$$\dot{\boldsymbol{r}} = \ddot{\boldsymbol{e}} + \boldsymbol{\alpha}\dot{\boldsymbol{e}} \tag{35}$$

where $\boldsymbol{\alpha} \in \mathbb{R}^{n \times n}$ is a diagonal, positive-definite, control gain matrix. Multiply by $\{\boldsymbol{F}^{+}\boldsymbol{M}\}$ both sides of the derivative of filtered tracking error dynamics given in (35) and insert the position tracking error and transformed (25) as follows:

$$\boldsymbol{F}^{+}\boldsymbol{M}\dot{\boldsymbol{r}} = \boldsymbol{F}^{+}\boldsymbol{M}(\ddot{\boldsymbol{z}}_d + \boldsymbol{\alpha}\dot{\boldsymbol{e}}) - \boldsymbol{u} + \boldsymbol{F}^{+}\boldsymbol{C}\dot{\boldsymbol{z}}_a + \boldsymbol{F}^{+}\boldsymbol{K}\boldsymbol{z}_a \tag{36}$$

From (36), the control input is proposed as

$$\boldsymbol{u} = \boldsymbol{F}^{+}\boldsymbol{M}(\ddot{\boldsymbol{z}}_d + \boldsymbol{\alpha}\dot{\boldsymbol{e}}) + \boldsymbol{F}^{+}\boldsymbol{C}\dot{\boldsymbol{z}}_a + \boldsymbol{F}^{+}\boldsymbol{K}\boldsymbol{z}_a + \boldsymbol{k}\boldsymbol{r} \tag{37}$$

where $\{\boldsymbol{F}^{+}\boldsymbol{M}(\ddot{\boldsymbol{z}}_d + \boldsymbol{\alpha}\dot{\boldsymbol{e}}) + \boldsymbol{F}^{+}\boldsymbol{C}\dot{\boldsymbol{z}}_a + \boldsymbol{F}^{+}\boldsymbol{K}\boldsymbol{z}_a\}$ is considered as feedforward term. From a control point of view, a feedback $\{\boldsymbol{kr}\}$ term is added to (37). Since the system parameters are treated as unknown, the composite adaptive controller formulation can be defined in a compact form of (37) as follows:

$$\boldsymbol{u} = \boldsymbol{Y}\hat{\boldsymbol{\Phi}} + \boldsymbol{k}\boldsymbol{r} \tag{38}$$

where $\boldsymbol{k} \in \mathbb{R}^{n \times n}$ is diagonal positive-definite control gain matrix and $\boldsymbol{Y} \in \mathbb{R}^{n \times p}$ a matrix of known functions.

4.3 Update rule

The update rule has a special format in the composite adaptive controller. The least-squares estimation method is used to generate an adaptive update rule. The least-squares update rule is defined as

$$\dot{\hat{\boldsymbol{\Phi}}} = \boldsymbol{\Gamma}\boldsymbol{W}_{\mathrm{f}}^{\mathrm{T}}\tilde{\boldsymbol{u}}_{\mathrm{f}} \tag{39}$$

In this case, $\boldsymbol{\Gamma} \in \mathbb{R}^{p \times p}$ is considered as a time-varying ($\boldsymbol{\Gamma}(t)$) and this symmetric matrix derivative defined as

$$\dot{\boldsymbol{\Gamma}} = -\boldsymbol{\Gamma}\boldsymbol{W}_{\mathrm{f}}^{\mathrm{T}}\boldsymbol{W}_{\mathrm{f}}\boldsymbol{\Gamma} \tag{40}$$

Note that using the matrix identity, the inverse of $\dot{\boldsymbol{\Gamma}}(t)$ is taken as $\dot{\boldsymbol{\Gamma}}^{-1} = \boldsymbol{W}_{\mathrm{f}}^{\mathrm{T}}\boldsymbol{W}_{\mathrm{f}}$. The infinite integral condition is to be defined to show the parameter update converge to their actual values. If

$$\lim_{t \to \infty} \lambda_{\min}\left\{\int_0^t \boldsymbol{W}_{\mathrm{f}}^{\mathrm{T}}(\sigma)\boldsymbol{W}_{\mathrm{f}}(\sigma)\,\mathrm{d}\sigma\right\} = \infty \tag{41}$$

then

$$\lim_{t \to \infty} \tilde{\boldsymbol{\Phi}} = 0 \tag{42}$$

The update rule for the composite adaptive controller is obtained by adding the least square term to the standard adaptive control update rule, which can be written as

$$\dot{\hat{\boldsymbol{\Phi}}} = \boldsymbol{\Gamma}\boldsymbol{Y}^{\mathrm{T}}\boldsymbol{r} + \boldsymbol{\Gamma}\boldsymbol{W}_{\mathrm{f}}^{\mathrm{T}}\tilde{\boldsymbol{u}}_{\mathbf{f}} \tag{43}$$

4.3.1 Theorem: The system (25), with the controller proposed in (38) and the parameter adaptation rule (43), ensures asymptotic converge of the error signal $e(t)$ and satisfies the infinite integral condition

$$\lim_{t \to \infty} \boldsymbol{e}(t) = 0 \tag{44}$$

4.3.2 Proof: We start our proof by proposing the following positive-definite function

$$V = \frac{1}{2}\boldsymbol{r}^{\mathbf{T}}\boldsymbol{F}^{+}\boldsymbol{M}\boldsymbol{r} + \frac{1}{2}\tilde{\boldsymbol{\Phi}}^{\mathrm{T}}\boldsymbol{\Gamma}^{-1}\tilde{\boldsymbol{\Phi}} \tag{45}$$

Differentiating the candidate Lyapunov function with respect to time and insert (36) with a control signal (38) in the derivative of the candidate function gives

$$\dot{V} = \boldsymbol{r}^{\mathrm{T}}\left(\boldsymbol{Y}\tilde{\boldsymbol{\Phi}} - \boldsymbol{k}\boldsymbol{r}\right) + \tilde{\boldsymbol{\Phi}}^{\mathrm{T}}\boldsymbol{\Gamma}^{-1}\dot{\tilde{\boldsymbol{\Phi}}} + \frac{1}{2}\tilde{\boldsymbol{\Phi}}^{\mathrm{T}}\dot{\boldsymbol{\Gamma}}^{-1}\tilde{\boldsymbol{\Phi}} \tag{46}$$

and make some arrangement with (40) and (43) gives

$$\begin{aligned}\dot{V} = {} & \boldsymbol{r}^{\mathrm{T}}\left(\boldsymbol{Y}\tilde{\boldsymbol{\Phi}} - \boldsymbol{k}\boldsymbol{r}\right) + \tilde{\boldsymbol{\Phi}}^{\mathrm{T}}\boldsymbol{\Gamma}^{-1}\left(-\boldsymbol{\Gamma}\boldsymbol{Y}^{\mathrm{T}}\boldsymbol{r} - \boldsymbol{\Gamma}\boldsymbol{W}_{\mathrm{f}}^{\mathrm{T}}\tilde{\boldsymbol{u}}_{\mathrm{f}}\right) \\ & + \frac{1}{2}\tilde{\boldsymbol{\Phi}}^{\mathrm{T}}\left(\boldsymbol{W}_{\mathrm{f}}^{\mathrm{T}}\boldsymbol{W}_{\mathrm{f}}\right)\tilde{\boldsymbol{\Phi}}\end{aligned} \tag{47}$$

Note that the adaptation term ($\boldsymbol{\Gamma}^{-1}$) is time varying, so its derivative is not zero. Finally, insert (33) and make a necessary arrangement, the derivative of candidate Lyapunov function turns

$$\dot{V} = -\boldsymbol{r}^{\mathrm{T}}\boldsymbol{k}\boldsymbol{r} - \frac{1}{2}\tilde{\boldsymbol{\Phi}}\boldsymbol{W}_{\mathrm{f}}^{\mathrm{T}}\boldsymbol{W}_{\mathrm{f}}\tilde{\boldsymbol{\Phi}} \tag{48}$$

$$\dot{V} \leq -\lambda_{\min}\{\boldsymbol{k}\} \parallel \boldsymbol{r} \parallel^2 \tag{49}$$

Now we can show that candidate function V is bounded. Since V is bounded, $\boldsymbol{F}^{+}\boldsymbol{M}$ is a positive-definite matrix, and $\boldsymbol{\Gamma}$ satisfies the infinite integral condition given in (41), we can state that r and $\tilde{\boldsymbol{\Phi}}$ is bounded. By the expression of filtered tracking error $\boldsymbol{e}$, $\dot{\boldsymbol{e}}$, $\boldsymbol{z}_a$, and $\dot{\boldsymbol{z}}_a$ are also bounded. In conclusion, the position tracking error e is asymptotically stable and the parameter error $\tilde{\boldsymbol{\Phi}}$ is also asymptotically stable if the finite integral condition is satisfied.

5 Experimental study

The designed control algorithm was implemented in the experimental set-up of the RMB flywheel system shown in Fig. 5. The Matlab/Simulink environment and dSpace MicroLabBox system are used for the controller implementation and data acquisition. Displacement signals of the flywheel generated from eddy current type non-contact sensors are provided to the digital control system through AD converters. The computed control currents are provided to the electromagnets through DA converters and power amplifiers. For the experiments, 25 kHz sampling frequency is used in the data acquisition system. To rotate the levitated flywheel system, a small air propeller attached to the top of the rotor. The laser tachometer was used to measure the rotational speed of the rotor. Note that the axial movement of the rotor is mechanically limit in ± 1 mm and radial movement is ± 1.5 mm, respectively.

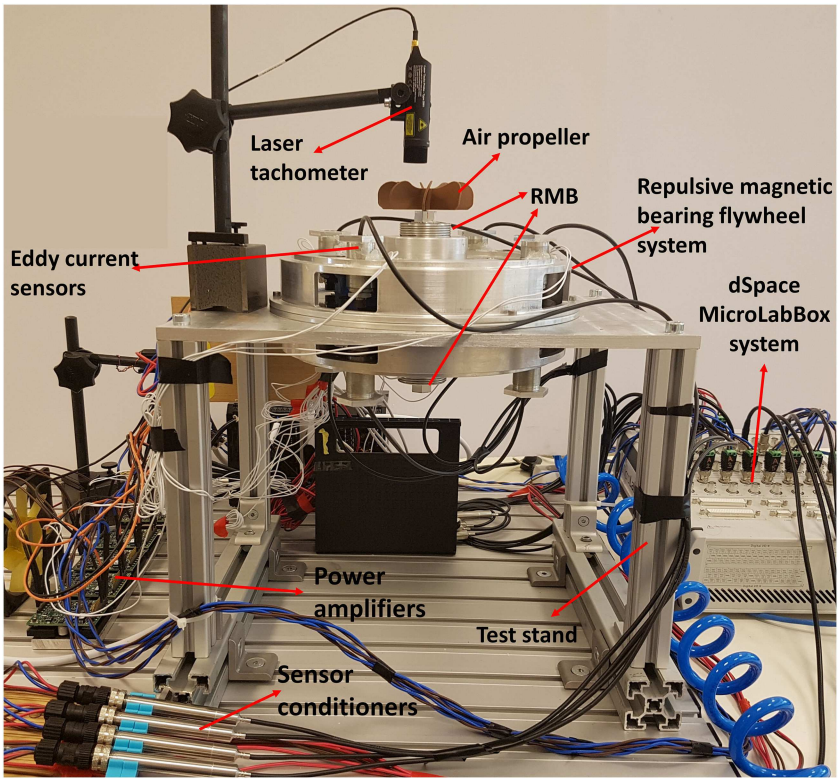

Fig. 5 *Experimental set-up of the flywheel system*

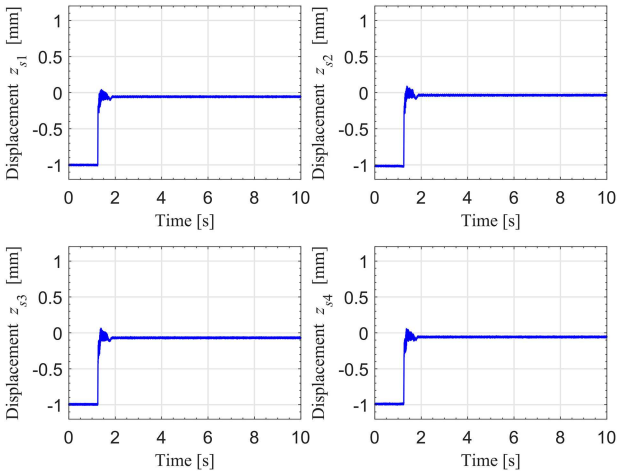

Fig. 6 *Displacements at the sensor locations z_{s1}, z_{s2}, z_{s3}, and z_{s4} for PID control*

5.1 PID control case

Firstly, a PID controller has been designed and applied to the experimental system in order to compare the effectiveness of the proposed composite adaptive controller.

Four local PID controller applied on the electromagnets. The parameters of the PID controller were decided as $P = 5$, $I = 25$, and $D = 0.02$ for all electromagnets after repeated precise tuning works. The displacements at the sensor locations of the flywheel are given in Fig. 6 and the control currents applied to the electromagnets in the levitation are also presented in Fig. 7. The experimental result shows that a steady-state error unavoidable in the case of conventional PID controller due to the model-independent control approach. On the other hand, it is observed that the parameter adaptation feature of the composite adaptive control is an advantage to force the steady-state error to zero.

5.2 Rotor levitation

The second experiment was carried out for the proposed control design to suspend the rotor to its set point location. It is aimed to levitate the rotor starting from an initial position to the zero-set point. The controller gains and adaptation rule gain matrix are selected to achieve the levitation of the rotor at minimum steady-state error as given below

$$\begin{aligned} \boldsymbol{\alpha} &= \mathrm{diag}\{6.2 \quad 6.2 \quad 6.2 \quad 6.2\} \\ \boldsymbol{k} &= \mathrm{diag}\{2000 \quad 2000 \quad 2000 \quad 2000\} \\ \boldsymbol{\Gamma}(0) &= \mathrm{diag}\{1.6\times10^{8} \quad 0.042 \quad 2\times10^{7} \quad 4\times10^{7}\} \end{aligned} \tag{50}$$

Fig. 8 shows the block diagram of the proposed composite adaptive controller scheme and parameter adaptation rule with integration. Note that adaptation rule gain matrix is the initial condition of the integral.

The flywheel was levitated with the composite adaptive controller and the displacements in the axial direction were obtained with eddy current sensors as shown in Fig. 9. The control currents applied to the electromagnets in the levitation are also presented in Fig. 10. The adaptations of the parameters are obtained as seen in Fig. 11. In the proposed controller, parameter adaptations start with certain initial values of the parameters and these values are decided some percentage of the nominal values such as $\boldsymbol{\Phi}(0) = 0.8\boldsymbol{\Phi}$. In experimental results, it is observed that the designed composite adaptive controller provides the improved position tracking error in transient performance and the fast parameter estimate convergence due to the least square-based adaptation formula. In magnetic levitation systems, the airgap is generally very small. As shown in Figs. 9 and 10, it appears that the levitation of four electromagnet location is very precise in the mid-air and the parameter adaptation is complete in almost 0.1 s.

5.3 Trajectory test

The controller performance was tested for the desired trajectory of the rotor rather than a zero-set point. In this case, the final values of the converged adaptation parameters were used in the experiment. In the proposed axial AMB structure, since each electromagnet is independent of each other, so it is possible to drive electromagnets with different currents. The following trajectory is defined for z_1 and z_3 electromagnets

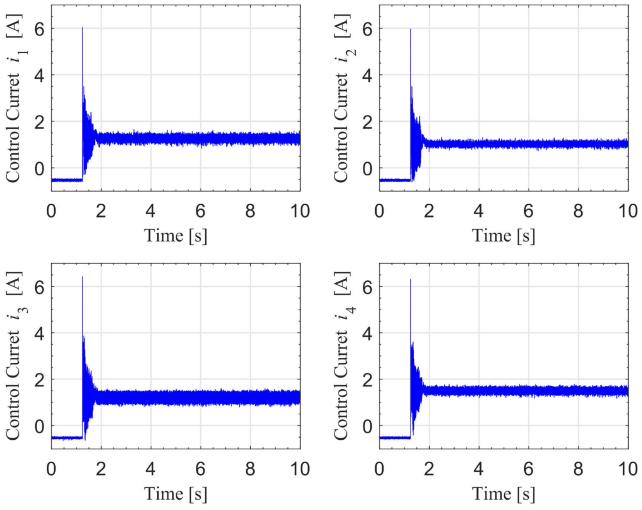

Fig. 7 *PID control currents applied to the electromagnets*

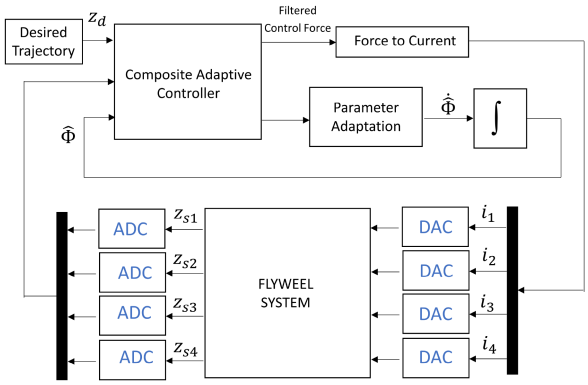

Fig. 8 *Block diagram of the proposed composite adaptive control scheme*

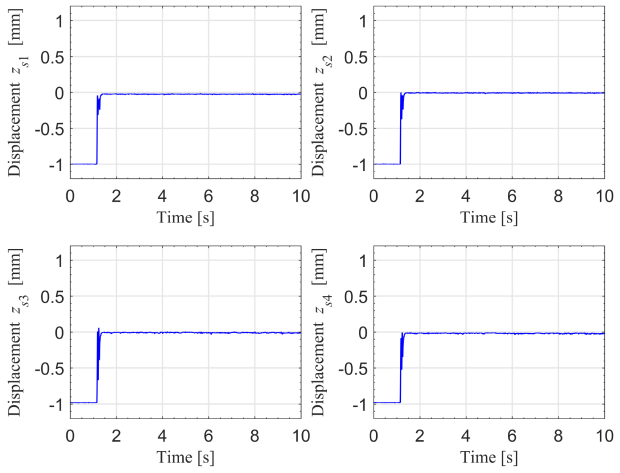

Fig. 9 *Displacements at the sensor locations z_{s1}, z_{s2}, z_{s3}, and z_{s4} for composite adaptive control*

$$
\begin{aligned}
z_{d1} &= 0.3 \times 10^{-3}\sin(4t) \\
z_{d2} &= 0 \\
z_{d3} &= 0.3 \times 10^{-3}\sin(4t + \pi) \\
z_{d4} &= 0
\end{aligned}
\tag{51}
$$

In these trajectory values, the flywheel was inclined to one side with a sine wave oscillation using the actively controlled electromagnet forces. While z_1 and z_3 locations oscillate, z_2 and z_4 locations are forced to hold zero displacements. The controller succeeded to follow the desired trajectory without disturbing the stability of the flywheel. Figs. 12 and 13 show the displacement

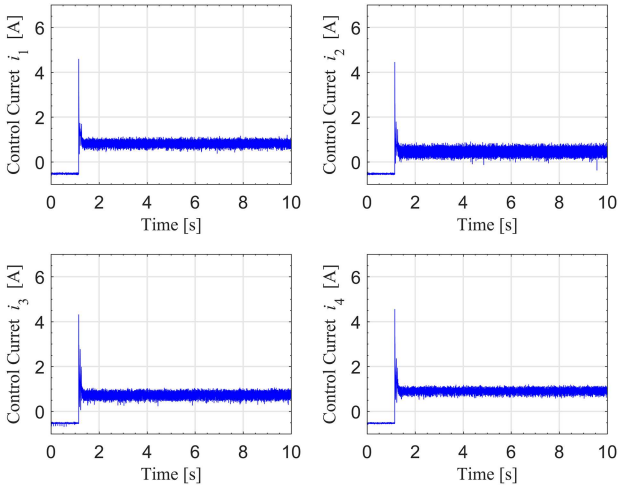

Fig. 10 *Composite adaptive control currents applied to the electromagnets*

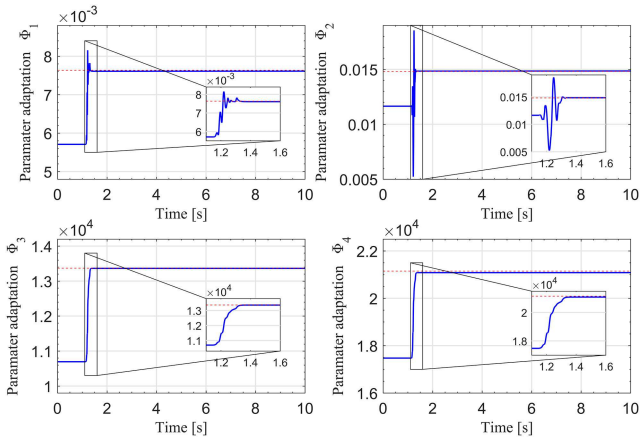

Fig. 11 *Parameter adaptations*

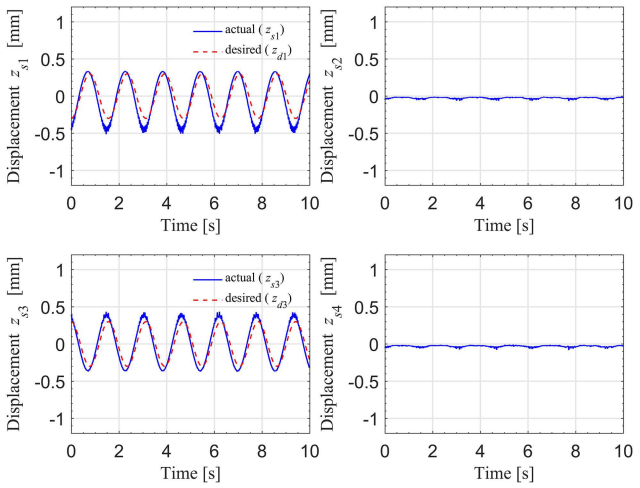

Fig. 12 *Displacements at the sensor locations z_{s1}, z_{s2}, z_{s3}, and z_{s4} with the desired trajectory for composite adaptive control*

results with the desired trajectory and the control currents, respectively.

The experiments were repeated for the same desired trajectory input at $\omega = 250$ rpm. Figs. 14 and 15 show the displacement results with the desired trajectory and control currents, respectively. Since air-jet used for rotation imposes large disturbance effect on the rotor the results obtained in experiment have some noise. However, obtained results are promising, the controller succeeded to follow the desired trajectory without interrupt the levitation of the flywheel.

One of the outputs of the trajectory test is that the proposed RMB flywheel system is suitable for small angular movements of

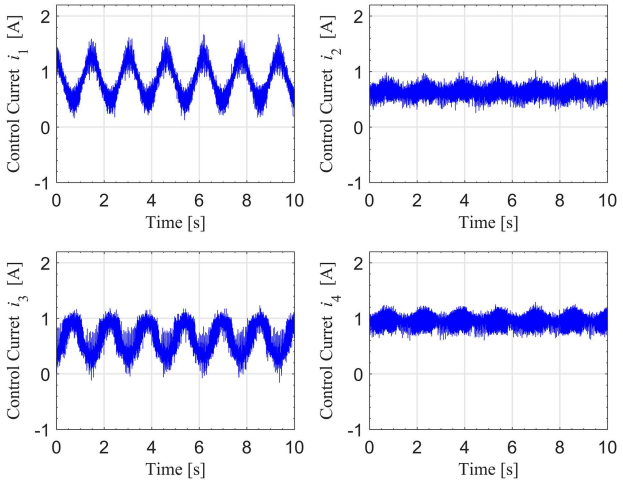

Fig. 13 *Composite adaptive control currents applied to the electromagnets*

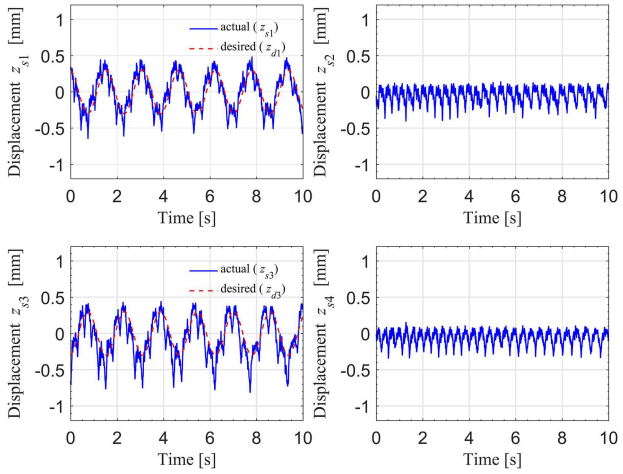

Fig. 14 *Displacements at the sensor locations z_{s1}, z_{s2}, z_{s3}, and z_{s4} with the desired trajectory for composite adaptive control at rotor speed $\omega = 250$ rpm*

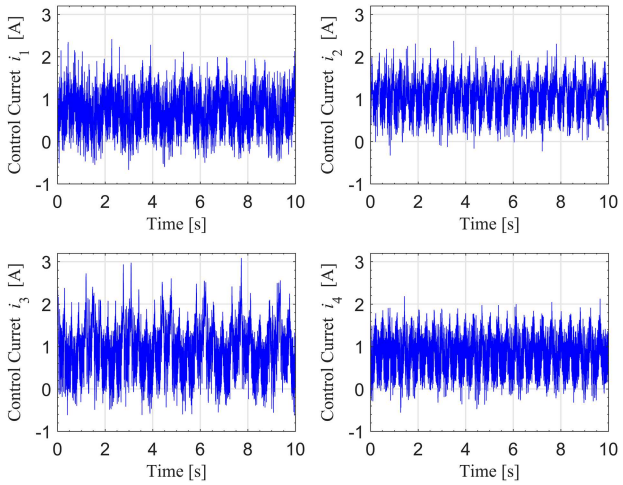

Fig. 15 *Composite adaptive control currents applied to the electromagnets at rotor speed $\omega = 250$ rpm*

the rotor. The spinning flywheel can be tilted using magnetic forces of the electromagnets in small degrees without contacting the magnetic bearings. The gap between the rotor and repulsive and active bearings makes the small tilting possible. This will create a small gimbaling effect in x and y directions and generate rotor-tilting torque for use potentially in an attitude control application.

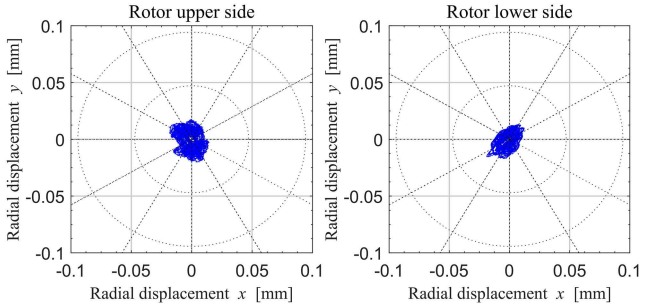

Fig. 16 *Orbits of the rotor at rotor speed $\omega = 250$ rpm*

5.4 Rotational test

In this case, a rotational test was realised to observe the performance of the controller in the effect of rotor dynamics. A simple air propeller is attached to the top of the rotor to perform a rotational experiment because an electric motor has not yet been assembled into the system for rotational movement of the rotor. Since air-jet imposes large disturbance effect on the rotor, the rotation of the flywheel is stopped at $\omega = 250$ rpm. To understand the radial dynamics of the rotor with repulsive bearings, the eddy current sensors are placed in the radial direction at the upper and lower positions (see Fig. 3). The measured radial displacements of the rotor in the upper and lower side can be drawn on the same plane. This type of representation is called the orbit of the rotor and shows the instant position of the rotor central axis during rotation. Small orbits diameter corresponds to the radial stability as given in Fig. 16.

6 Conclusion

In this research work, the design of a full state feedback composite adaptive controller is presented for a novel RMB flywheel system. The unstable magnetic forces due to RMBs impose extra loads on the active control system in the flywheel structure. The experimental results showed that the proposed composite adaptive controller provided good convergence to desired trajectory and parameter estimation under the effect of the magnetic disturbance forces and moments. The flywheel system is also suitable for the desired trajectory application. It may be used potentially for attitude control in a spacecraft as a momentum exchange device which prefers the desired trajectory rather than setpoint problem. Moreover, the composite adaptive controller has faster parameter estimate convergence. Experiment results were presented to illustrate the effectiveness of the composite adaptive controller with different cases including rotational results.

7 Acknowledgment

This work was supported by The Scientific and Technological Research Council of Turkey through grant no 214M284 under the research projects funding program.

8 References

[1] Sidi, M.J.: '*Spacecraft dynamics and control: a practical engineering approach*' (Cambridge University Press, UK, 1997)

[2] Wang, X., Han, C., Yu, Y., *et al.*: 'A modified adaptive backstepping method for shaft deflection tracking control of magnetically suspended momentum wheel with nonlinear magnetic torque', *J. Franklin Inst.*, 2018, **355**, (7), pp. 3274–3287

[3] Li, X., Palazzolo, A.: 'Multi-input–multi-output control of a utility-scale, shaftless energy storage flywheel with a five-degrees-of-freedom combination magnetic bearing', *J. Dyn. Syst. Meas. Contr.*, 2018, **140**, p. 101008-1

[4] Li, X., Anvari, B., Palazzolo, A., *et al.*: 'A utility-scale flywheel energy storage system with a shaftless, hubless, high strength steel rotor', *IEEE Trans. Ind. Electron.*, 2018, **65**, (8), pp. 6667–6675

[5] Chiba, A., Fukao, T., Ichikawa, O., *et al.*: '*Magnetic bearings and bearingless drives*' (Elsevier, Netherlands, 2005)

[6] Wang, D., Wang, N., Ye, C., *et al.*: 'Research on analytical bearing capacity model of active magnetic bearings based on magnetic saturation', *IET Electr. Power Appl.*, 2017, **11**, (9), pp. 1548–1557

[7] Ran, S., Hu, Y., Wu, H.: 'Design, modeling, and robust control of the flexible rotor to pass the first bending critical speed with active magnetic bearing', *Adv. Mech. Eng.*, 2018, **10**, (2), pp. 1–13

[8] Zhong, W., Palazzolo, A., Kang, X.: 'Multi-objective optimization design of nonlinear magnetic bearing rotordynamic system', *J. Vib. Acoust.*, 2017, **139**, (1), p. 011011
[9] Kandil, M., Dubois, M.R., Bakay, L., *et al.*: 'Application of second-order sliding mode concepts to active magnetic bearings', *IEEE Trans. Ind. Electron.*, 2018, **65**, (1), pp. 855–864
[10] Jiancheng, F., Jinji, S., Hu, L., *et al.*: 'A novel 3-DOF axial hybrid magnetic bearing', *IEEE Trans. Magn.*, 2010, **46**, (12), pp. 4034–4045
[11] Zad, H.S., Khan, T.I., Lazoglu, I.: 'Design and adaptive sliding-mode control of hybrid magnetic bearings', *IEEE Trans. Ind. Electron.*, 2018, **65**, (3), pp. 2537–2547
[12] Santra, T., Roy, D., Choudhury, A.B., *et al.*: 'Vibration control of a hybrid magnetic bearing using an adaptive sliding mode technique', *J. Vib. Control*, 2018, **24**, (10), pp. 1848–1860
[13] Mukhopadhyay, S.C., Donaldson, J., Sengupta, G., *et al.*: 'Fabrication of a repulsive-type magnetic bearing using a novel arrangement of permanent magnets for vertical-rotor suspension', *IEEE Trans. Magn.*, 2003, **39**, (5), pp. 3220–3222
[14] Inoue, T., Sugai, T., Ishida, Y.: 'Vibration suppression of the rotating shaft using the axial control of the repulsive magnetic bearing', *J. Syst. Des. Dyn.*, 2010, **4**, (4), pp. 575–589
[15] Paden, B., Groom, N., Antaki, J.F.: 'Design formulas for permanent-magnet bearings', *J. Mech. Des.*, 2003, **125**, (4), pp. 734–738
[16] Marth, E., Jungmayr, G., Panholzer, M., *et al.*: 'Optimization and realization of a multi-pole permanent magnetic bearing with rotating magnetization', *Proc. Inst. Mech. Eng., Part I: J. Syst. Contr. Eng.*, 2016, **230**, (4), pp. 320–329
[17] Safaeian, R., Heydari, H.: 'Comprehensive comparison of different structures of passive permanent magnet bearings', *IET Electr. Power Appl.*, 2017, **12**, (2), pp. 179–187
[18] Siebert, M., Ebihara, B., Jansen, R., *et al.*: 'A passive magnetic bearing flywheel'. Intersociety Energy Conversion Engineering Conf. SAE, Savannah, USA, May 2001, pp. 125–132
[19] Filatov, A.V., Maslen, E.H.: 'Passive magnetic bearing for flywheel energy storage systems', *IEEE Trans. Magn.*, 2001, **37**, (6), pp. 3913–3924
[20] Bassani, R.: 'Passive magnetic bearing for flywheel energy storage systems', *Nonlinear Dyn.*, 2007, **50**, (1), pp. 161–168
[21] Ohji, T., Katsuda, Y., Amei, K., *et al.*: 'Structure of one-axis controlled repulsive type magnetic bearing system with surface permanent magnets installed and its levitation and rotation tests', *IEEE Trans. Magn.*, 2011, **47**, (12), pp. 4734–4739
[22] Bassani, R.: 'Stability of permanent magnet bearings under parametric excitations', *Tribol. Trans.*, 2005, **48**, (4), pp. 457–463
[23] Hussien, A.A., Yamada, S., Iwahara, M., *et al.*: 'Application of the repulsive-type magnetic bearing for manufacturing micromass measurement balance equipment', *IEEE Trans. Magn.*, 2005, **41**, (10), pp. 3802–3804
[24] Mukhopadhyay, S.C.: 'Modeling of a repulsive type magnetic bearing for five axis control under intermittent operation including eddy current effect'. Proc. 1st IEEE Int. Workshop on Electronic Design, Test and Applications, Christchurch, New Zealand, 2002, pp. 425–427
[25] Sivrioglu, S.: 'Adaptive control of nonlinear zero-bias current magnetic bearing system', *Nonlinear Dyn.*, 2007, **48**, (1), pp. 175–184
[26] Lewis, F.L., Dawson, D.M., Abdallah, C.T.: '*Robot manipulator control: theory and practice*' (CRC Press, USA, 2003)
[27] Krstic, M., Kanellakopoulos, I., Kokotovic, P.V.: '*Nonlinear and adaptive control design*' (Wiley, USA, 1995)